Science Advances
AAAS

advances.sciencemag.org/cgi/content/full/6/30/eaaz9708/DC1

Supplementary Materials for

Direct observation of anisotropic growth of water films on minerals driven by defects and surface tension

Sibel Ebru Yalcin*, Benjamin A. Legg, Merve Yeşilbaş, Nikhil S. Malvankar*, Jean-François Boily*

*Corresponding author. Email: jean-francois.boily@umu.se (J.-F.B.); sibel.yalcin@yale.edu (S.E.Y.); nikhil.malvankar@yale.edu (N.S.M.)

Published 24 July 2020, *Sci. Adv.* **6**, eaaz9708 (2020)
DOI: 10.1126/sciadv.aaz9708

The PDF file includes:

Other Supplementary Material for this manuscript includes the following:

(available at advances.sciencemag.org/cgi/content/full/6/30/eaaz9708/DC1)

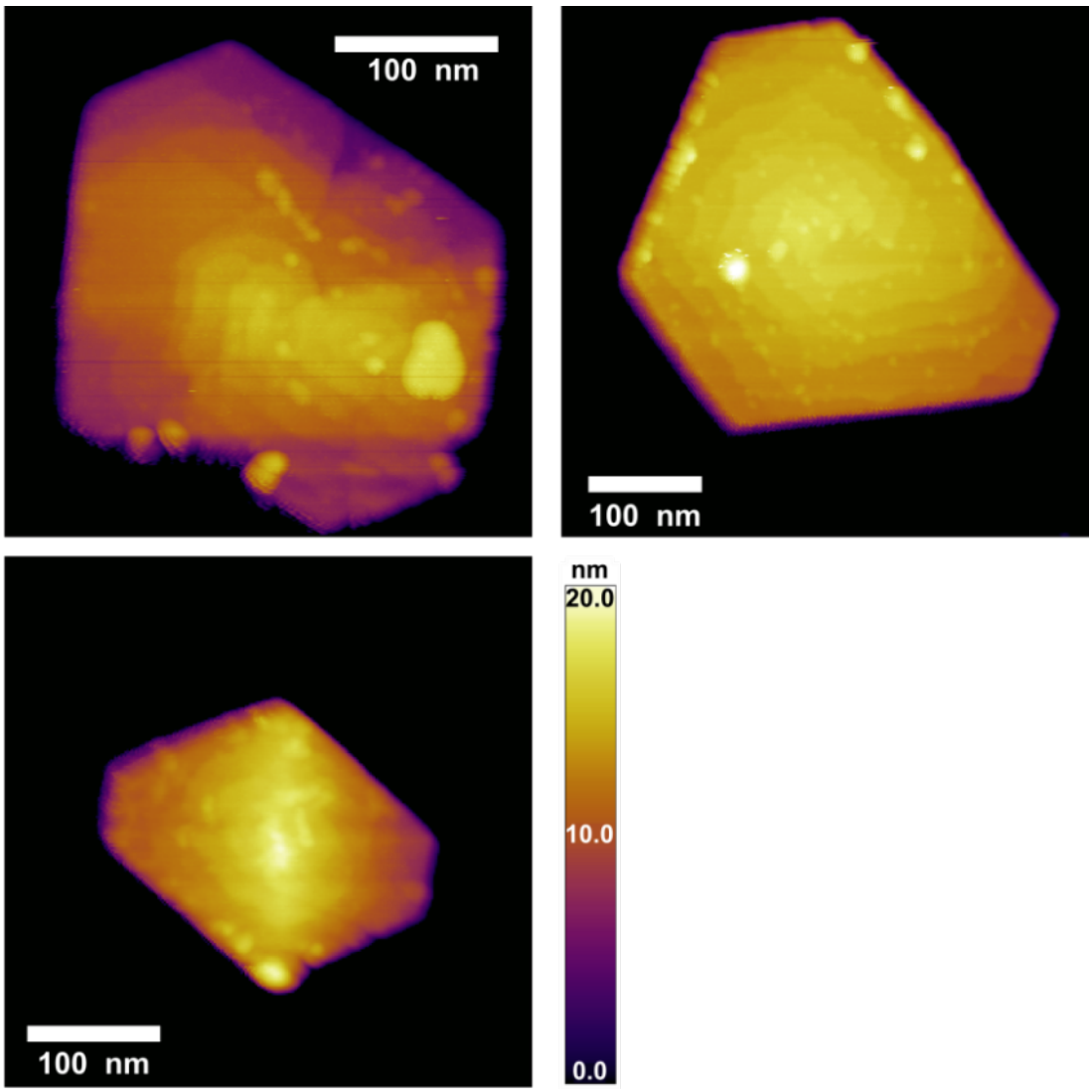

Figure S1. **AFM topography images of various gibbsite nanoparticles showing surface defects, including spiral-growth features.** Similar surface morphologies and defects are also apparent on gibbsite platelets shown in Figs. 1B and 3A.

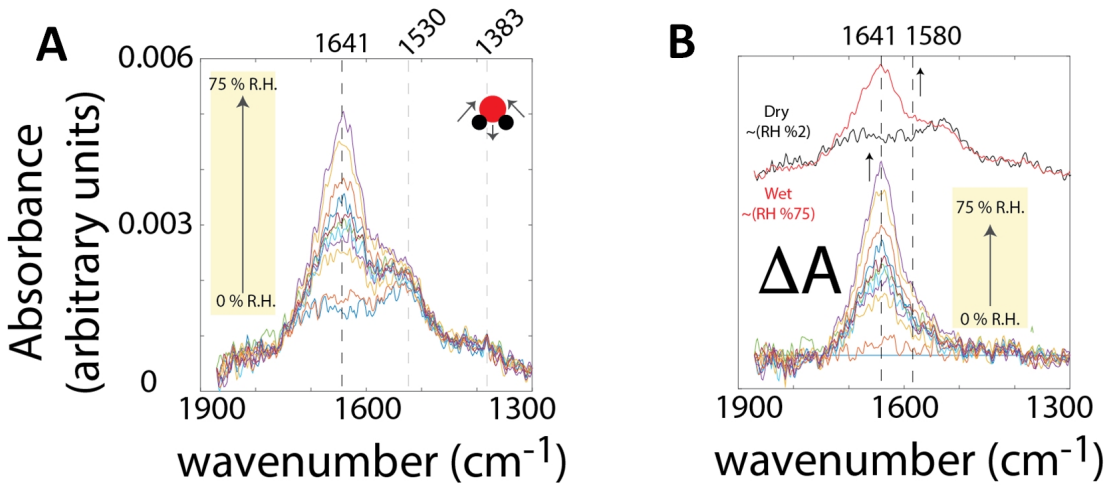

Figure S2. **ATR-FTIR spectra of gibbsite exposed to 0-75 % RH at 25 °C, revealing the deposition of a liquid water film.** Water bending region showing **(A)** the total and **(B)** the different spectra. The difference spectra in the water bending region is a sensitive measure of water film growth upon exposure of water vapor to gibbsite. Water vapor lines are generally undetected in ATR-FTIR mode as the sample covers the entire analytical region.

,

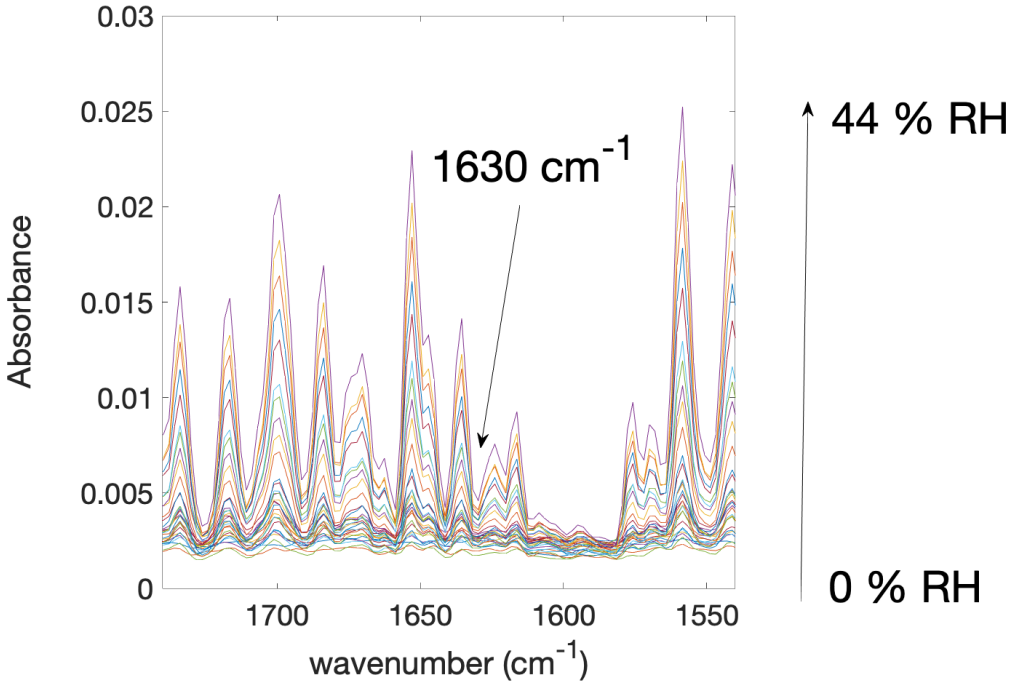

Figure S3. **Transmission spectra of water bending region.** IR *s*-SNOM work at 1630 cm^{-1} enhances signal from mineral-bound water film while avoiding narrow band of water vapor around 1640cm^{-1}. (Fig. S2)

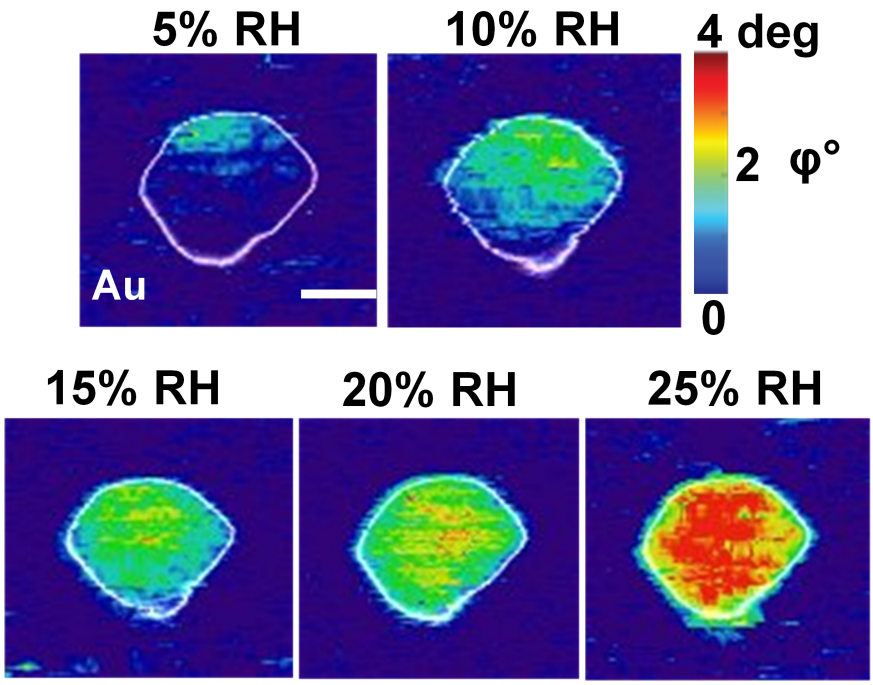

Figure S4. Topography superimposed SNOM phase images showing anisotropic water growth on gibbsite starting from the edge of mineral. Topography shown here as a white boundary is also presented separately in Fig. 2D. Representative IR *s*-SNOM phase images are collected at 1630 cm^{-1} with varying RHs shown in Fig. 2D. In this figure we aligned the SNOM images shown in Fig. 2D to keep the mineral in the centre of the image. Scale bar is 200 nm. IR s-SNOM scan direction is from top to bottom.

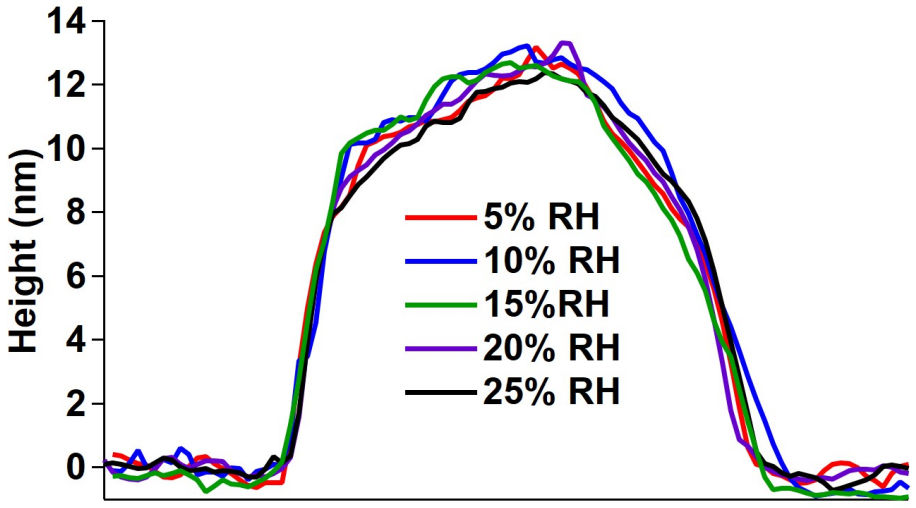

Figure S5. **Topographical cross-sections of the Gibbsite particle** used for IR s-SNOM studies shown in Fig. 2C as a varying RH collected in the adsorption regime.

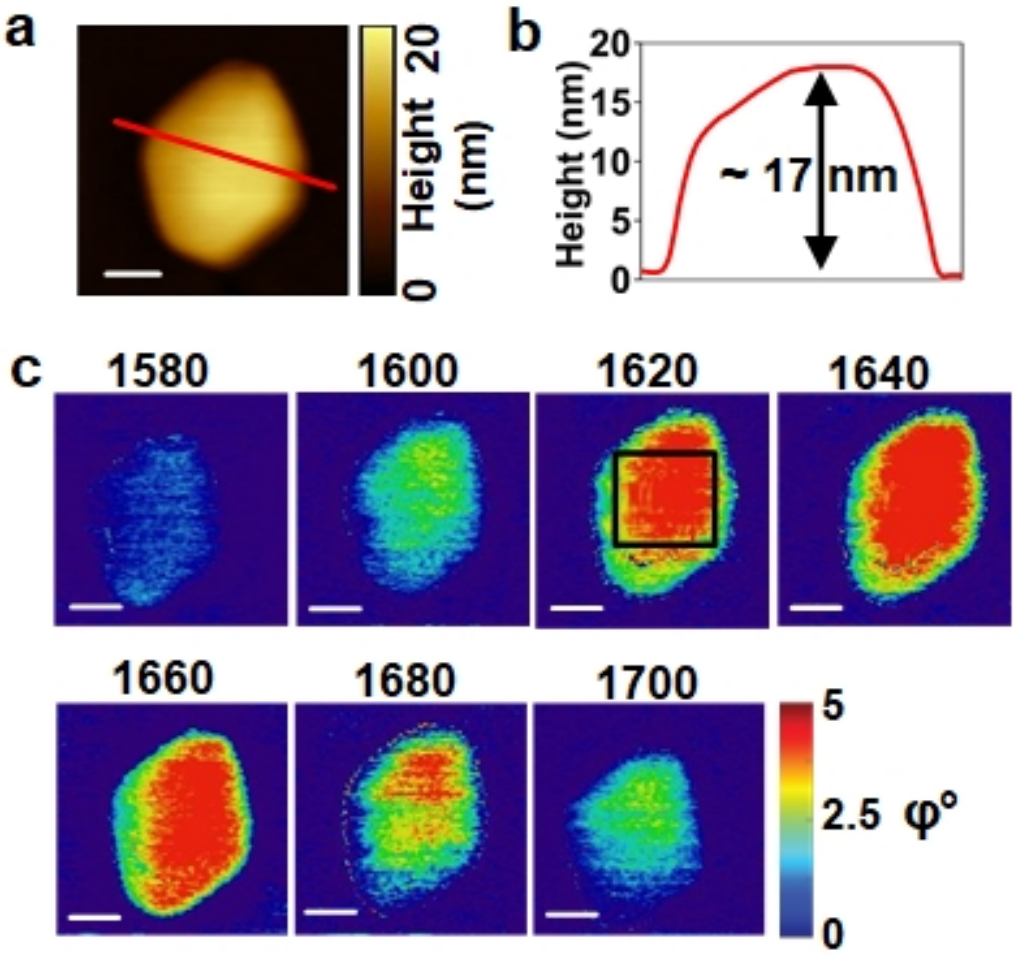

Figure S6. **Nanoscale IR spectra on individual gibbsite nanoparticle recorded from 1590 to 1700 cm^{-1} reveals that OH water bending signal is enhanced around 1640 cm^{-1}. (A)** AFM topography and **(B)** corresponding height cross section to Gibbsite nanoparticle. **(C)** Repetitive SNOM phase images (representing $3\omega_t$ demodulation) on Gibbsite nanoparticle. The corresponding wavenumber values (in unit cm^{-1}) are given on the top of each figure. Scale bar is 200 nm in (A) and (C). Square black region corresponds to 50 px by 50 px selected region from each collected wavenumber images for the mineral. The details of statistical analysis to extract the spectra is mentioned in Methods and the spectra of individual gibbsite mineral is shown in Fig. 2B, blue dots that agrees very well with the bulk FTIR spectra collected from mineral powders shown in Fig. 2B, black line.

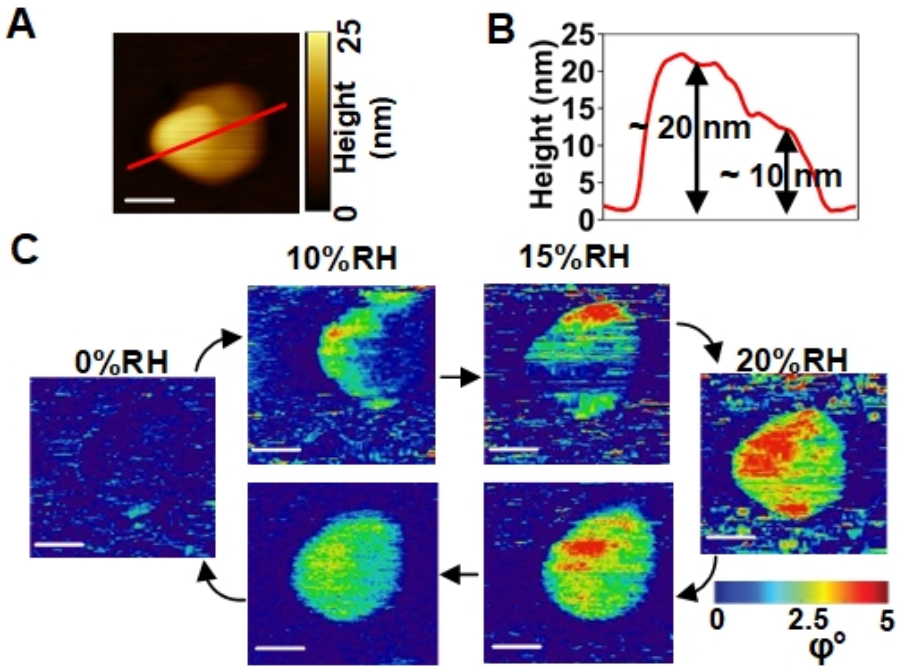

Figure S7. IR s-SNOM images showing reversibility of water uptake. Arrows indicate direction of increasing and decreasing RH recorded at 1630 cm^{-1} corresponding to water bending mode. SNOM data are representing $3\omega_t$ demodulation. IR s-SNOM scan direction is from top to bottom. Scale bars in (A) and (C) are 200 nm.

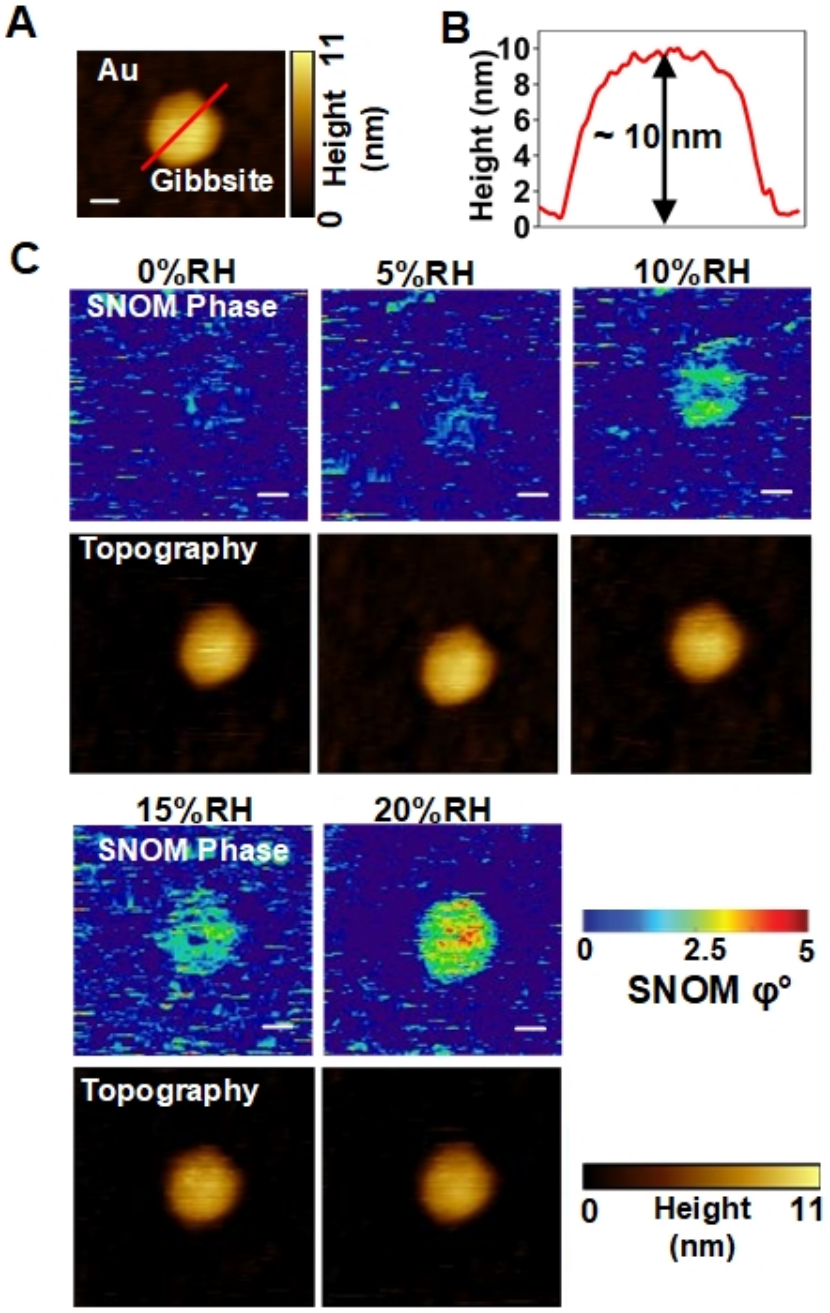

Figure S8. Repeat measurements of IR *s*-SNOM imaging on another individual gibbsite nanoparticle recorded at water bending mode (1630 cm^{-1}) at adsorption regime reveals similar anisotropic water uptake. (A) AFM topography **(B)** corresponding height cross section of gibbsite nanoparticle. **(C)** Representative water absorption images of gibbsite as a varying RH shown together with its simultaneously recorded topography images. The SNOM data is collected using $2\omega_t+\Omega_r$ demodulation. ($\omega_t \sim 330$ kHz and Ω_r is the frequency of the chopper used in the reference arm, $\Omega_r << \omega_t$). Scale bars in (a) and (c) are 100 nm. IR s-SNOM scan direction is from top to bottom.

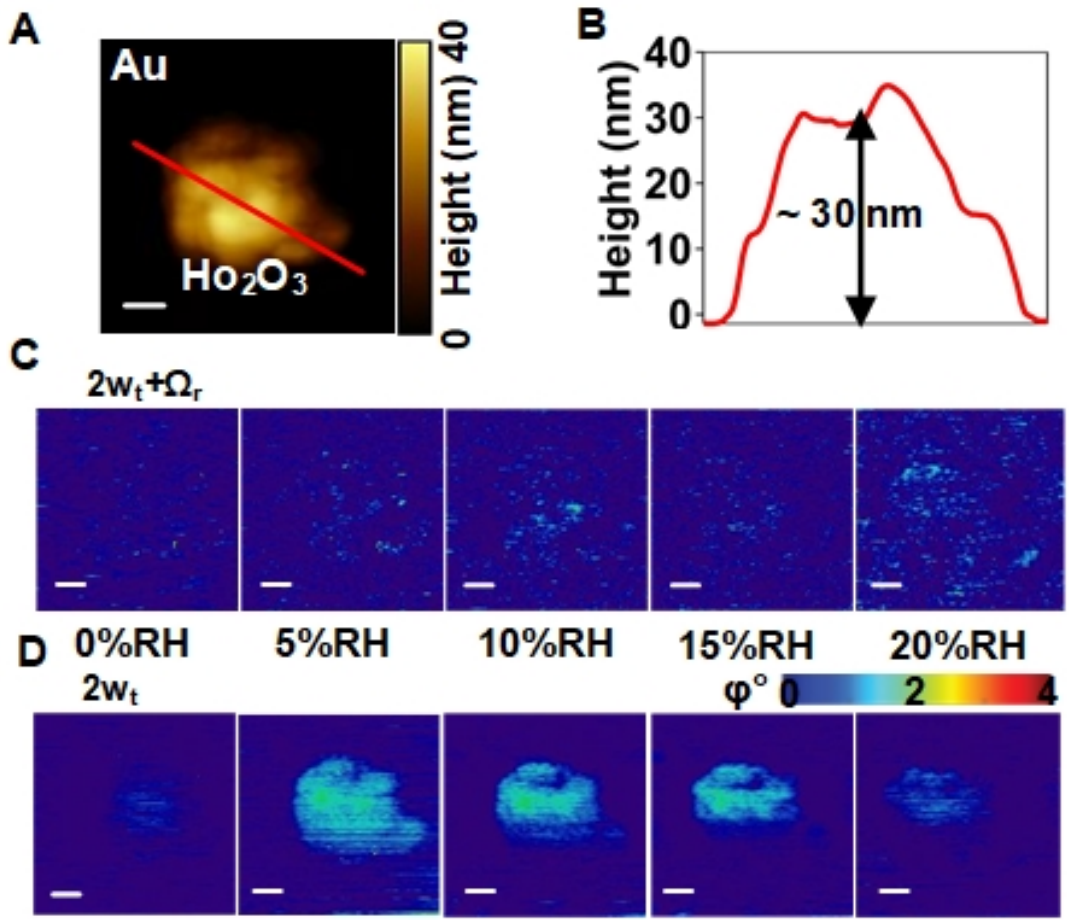

Figure S9. IR *s*-SNOM control experiments on individual hydrophobic rare earth oxide particles at the *adsorption regime* reveals almost none to very low water uptake suggesting the requirement of hydrophilic surface for water film growth. (A) SNOM topography of the single Holmium Oxide (Ho_2O_3) nanoparticle and **(B)** Corresponding height cross section for the red line shown in (A). **(C)** IR *s*-SNOM phase images collected at 1630 cm^{-1} on Ho_2O_3 using $2\omega_t+\Omega_r$ demodulation (ω_t ~ 330 kHz and Ω_r is the frequency of the chopper used in the reference arm, $\Omega_r << \omega_t$) showing no growth of water film as the RH is increased. **(D)** IR *s*-SNOM phase images collected at 1630 cm^{-1} on holmium oxide using $2\omega_t$ demodulation showing small variation in the phase contrast (<1°). The overall water uptake on these Ho_2O_3 particles are much lower (at least 3-4 times) compared to the gibbsite platelets (Fig. 3A) suggesting that these particles are indeed hydrophobic and water film could not grow over the Ho_2O_3 even at 20% RH. Scale bars in (A), (C) and (D) are 200 nm.

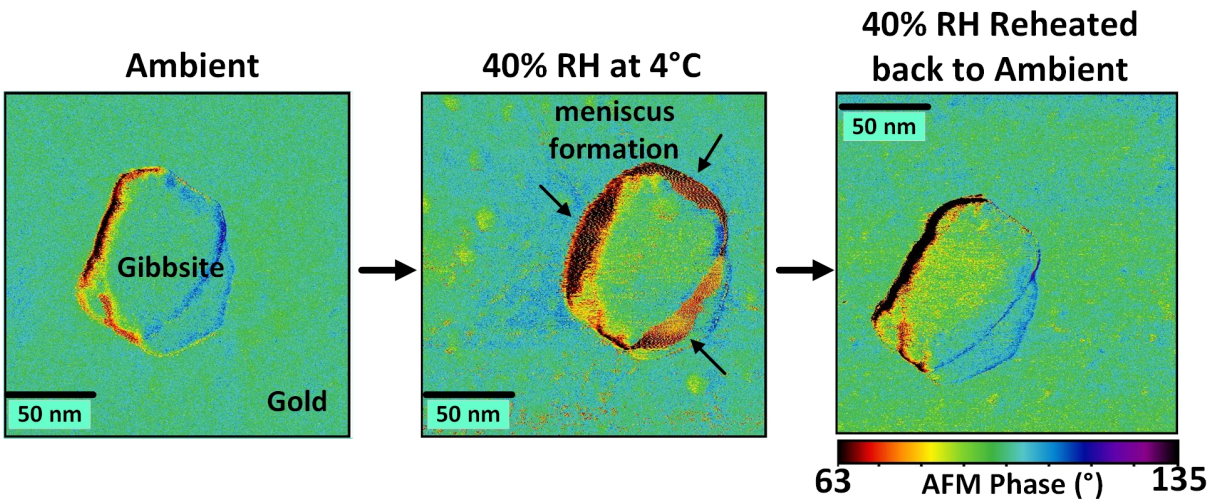

Figure S10. AFM phase images of gibbsite mineral show the formation of edge meniscus at 4°C. The height profile of the same gibbsite nanoparticle is presented in Fig. 4. AFM shows the recorded series of AFM phase images on this particle as the sample temperature is reduced from ambient to 4°C and then heated back to ambient temperature. AFM phase images clearly show the condensed water and the edge meniscus formed on the gibbsite mineral at 40 % RH of 4° C.

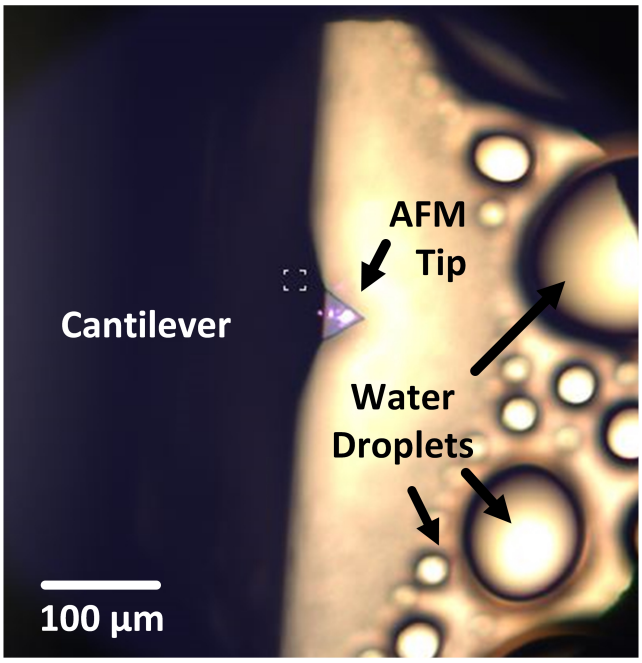

Figure S11. Water droplets were formed at 4°C in the condensation regime. Optical image of sample and the AFM tip taken through Cypher AFM camera when the sample temperature was reduced to 4 °C. We see the effect of increased humidity and condensation in the sample chamber, causing large water droplet formation over the sample surface.

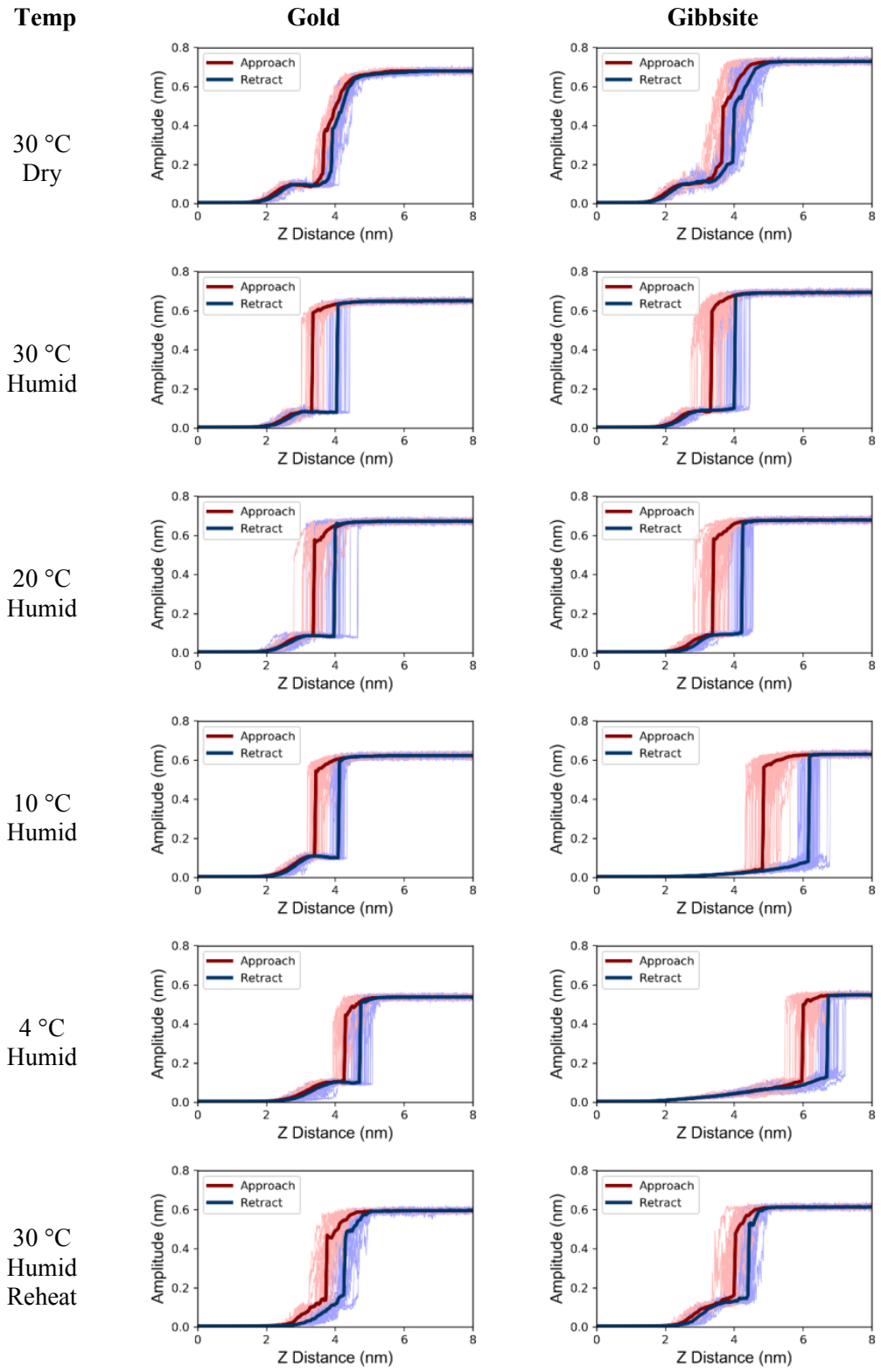

Figure S12. AFM amplitude curves on gold (left) and gibbsite (right). Pink and light blue curves represent the individual curves. Bold red and dark blue curves represent the averages for approach and retract respectively.

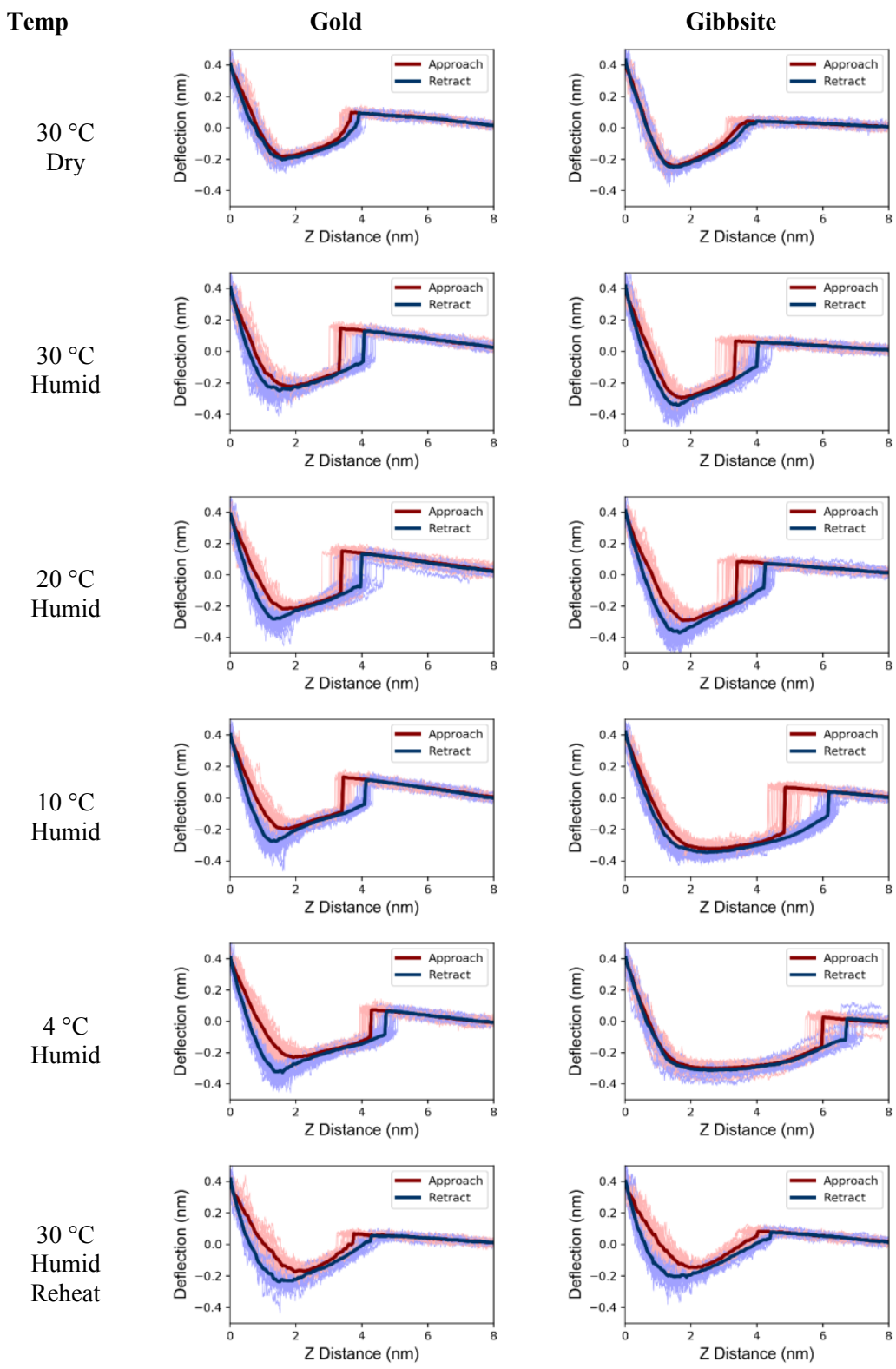

Figure S13. AFM deflection curves on gold (left) and gibbsite (right). Pink and light blue curves represent the individual curves. Bold red and dark blue curves represent the averages for approach and retract respectively.

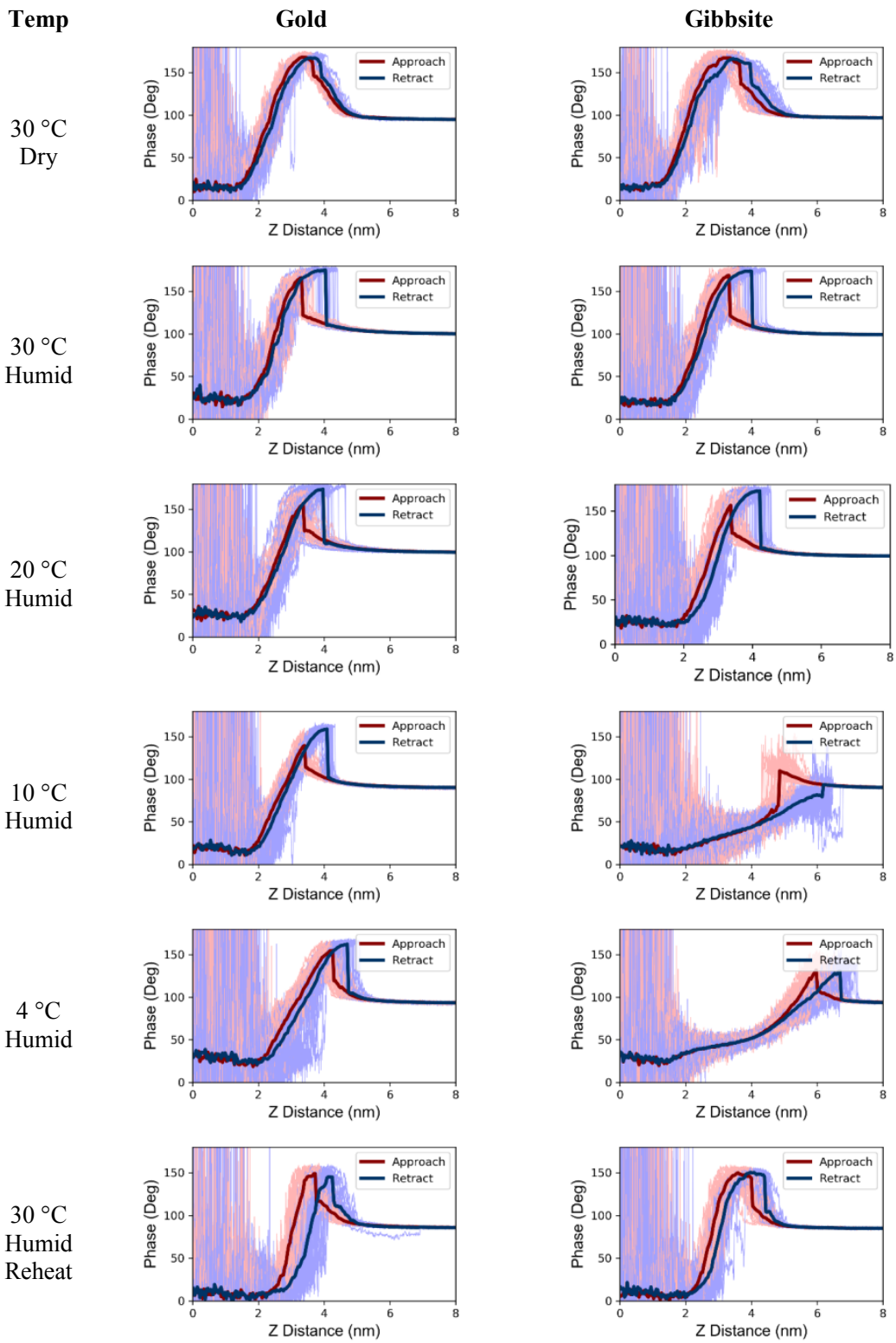

Figure S14. AFM phase curves on gold (left) and gibbsite (right). Pink and light blue curves represent the individual curves. Bold red and dark blue curves represent the averages for approach and retract respectively.

	Gibbsite Approach (nm)		Gibbsite Retract (nm)		Gold Approach (nm)		Gold Retract (nm)	
Condition	Avg	Std	Avg	Std	Avg	Std	Avg	Std
Dry Argon	3.10	0.36	3.41	0.29	3.48	0.70	3.62	0.67
30°C	2.80	0.29	3.53	0.27	2.86	0.29	3.38	0.32
20°C	2.98	0.33	3.87	0.25	2.96	0.24	3.62	0.32
10°C	4.37	0.41	5.70	0.27	3.04	0.20	3.83	0.26
4°C	5.44	0.72	6.32	0.91	3.70	0.36	4.13	0.37
30°C (Reheat)	3.88	0.82	4.31	0.80	3.24	0.27	3.74	0.32

Table S1. Statistics, generated from the force curves in Fig. 4, showing the average changes in the tip-sample distance during tip approach and retraction. When we reheat the sample to 30°C, the observed recovery in the distances prove that the measured changes are due to the changes in the humidity/temperature. Each value is estimated based on a minimum of 80 force curves. We see almost full recovery in the distances from the gold surface, however the recovery from the gibbsite surface is not 100%. This is presumably due to tip-water interaction that causes irreversible change on the tip during repetitive scans.

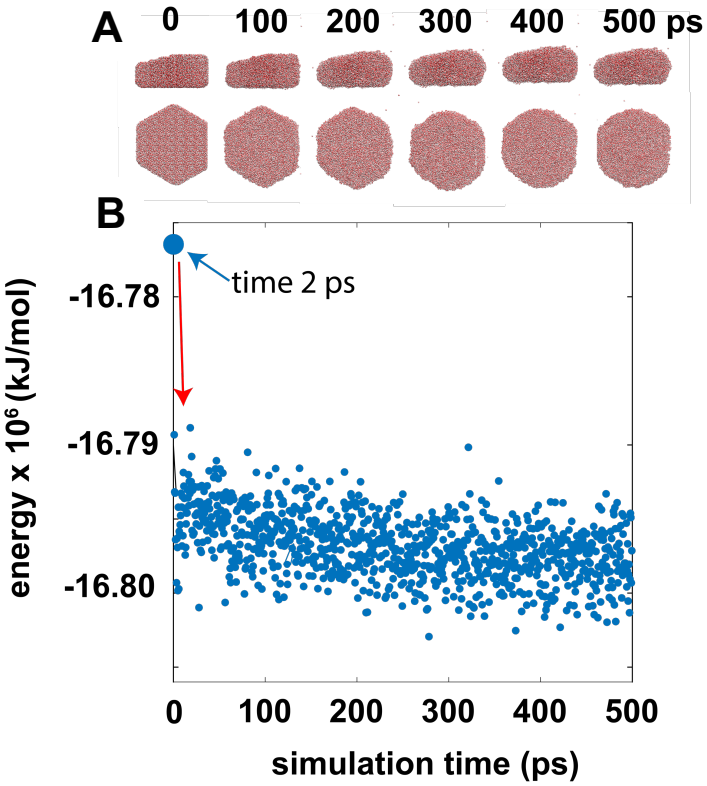

Figure S15. Molecular dynamics simulations of roughened 112 × 47 nm gibbsite nanoparticle initially covered with a film of homogeneous thickness at d=1.00 nm. Here are shown in **(A)** morphologies of the films at selected simulation times, and **(B)** the total energy of the simulation cell in the first 500 ps. Films departed from the initial gibbsite morphology to decrease the total surface area, a means to minimise the surface energy. This effectively increases water loadings over the central parts of the faces and depletes them at the edges. Simulations were run at a time step of 0.5 fs in an isothermal–isobaric (NPT) ensemble at 300 K.